Received: 13 April 2018 | Accepted: 22 May 2018

DOI: 10.1111/jace.15798

Check for updates

Journal of the American Ceramic Society

RAPID COMMUNICATION

Potential thermal barrier coating materials: RE_3NbO_7 (RE=La, Nd, Sm, Eu, Gd, Dy) ceramics

Lin Chen | **Peng Wu** | **Peng Song** | **Jing Feng**

Faculty of Material Science and Engineering, Kunming University of Science and Technology, Kunming, China

Correspondence
Jing Feng, Faculty of Material Science and Engineering, Kunming University of Science and Technology, Kunming, China.
Email: vdmzsfj@sina.com

Funding information
young-talent support programs of Kunming University of Science and Technology, Grant/Award Number: 11504146; National Natural Science Foundation of China, Grant/Award Number: 51762028

Abstract

In this work, RE_3NbO_7 ceramics are synthesized via solid-state reaction and the phase structure is characterized by X-ray diffraction and Raman spectroscopy. The relationship between crystal structure and thermophysical properties is determined. Except Sm_3NbO_7, each RE_3NbO_7 exhibits excellent high-temperature phase stability. The thermal expansion coefficients increase with the decreasing RE^{3+} ionic radius, which depends on the decreasing crystal lattice energy and the maximum value reaches 11.0 × 10^{-6} K^{-1} at 1200°C. The minimum thermal conductivity of RE_3NbO_7 reaches 1.0 W m^{-1} K^{-1} and the glass-like thermal conductivity of Dy_3NbO_7 is dominant by the high concentration of oxygen vacancy and the local structural order. The outstanding thermophysical properties pronounce that RE_3NbO_7 ceramics are potential thermal barrier coating materials.

KEYWORDS

fluorite, rare-earth niobates, thermal barrier coatings, thermal conductivity, thermal expansion

1 | INTRODUCTION

Thermal barrier coatings (TBCs) are applied in advanced gas turbines and aircraft engines to provide thermal insulation for high-temperature components and improve the oxidation and corrosion resistance.[1–4] Nowadays, commercial TBCs are yttria-stabilized zirconia (6-8 wt% YSZ), which exhibits the remarkable thermophysical and mechanical properties.[5,6] YSZ exhibits relatively low thermal conductivity (2.1-3.0 W m^{-1} K^{-1}, 25-1000°C), high thermal expansion coefficients (10.0 × 10^{-6} K^{-1}, 1200°C), excellent high-temperature toughness and low Young's modulus.[6,7] Nevertheless, the application temperature of YSZ is below 1200°C as the phase transition over 1200°C will lead to volume expansion and then fail the coatings.[8,9] Furthermore, high sintering rate of YSZ will cause the increase of Young's modulus and thermal conductivity.[7] Therefore, numerous ceramics are investigated to replace YSZ and increase the application temperature of TBCs. Among various ceramics, the compounds with fluorite-type crystal structure such as rare-earth zirconates ($RE_2Zr_2O_7$, RE, rare-earth elements),[10,11] lanthanum cerium oxides ($La_2Ce_2O_7$)[12] and rare-earth tantalates are the most investigated materials.[13–15] The merits of fluorite-type ceramics include low thermal conductivity, excellent high-temperature phase stability, outstanding toughness and relatively high hardness. Besides, multifarious methods are applied to optimize the comprehensive properties of fluorite-type ceramics.

The mechanical and thermal properties of $La_2Zr_2O_7$ ceramics are optimized via Yb substitution.[16] The thermal radiation effect of $La_2Zr_2O_7$ ceramics is effectively blocked by the addition of $LaPO_4$.[17] Ti is applied to substitute Zr in $La_2Zr_2O_7$ and the thermal conductivity is reduced effectively.[18] It is important to note that $Sm_2Zr_2O_7$ is applied in G level gas turbine with 1500°C operation temperature. One can see that fluorite-type ceramics are potential TBCs. Besides $RE_2Zr_2O_7$, $La_2Ce_2O_7$ and RE_3TaO_7, there is another kind of fluorite-type ceramics, that is, rare-earth niobates RE_3NbO_7.[19] Normally, researchers focus on the crystal structure and dielectric properties of RE_3NbO_7, the thermophysical properties such as thermal conductivity and thermal expansion coefficients of these ceramics are restricted.[20–22]

In this work, we focus on the relationship between crystal structure and thermophysical properties of RE_3NbO_7

 © 2018 The American Ceramic Society

(RE=La, Nd, Sm, Eu, Gd, Dy) ceramics. The properties including Vickers hardness, fracture toughness, specific heat, thermal diffusivity, thermal conductivity, thermal expansion coefficients and high-temperature phase stability are studied. It is proposed that RE_3NbO_7 ceramics are potential TBC materials contributed to the outstanding thermophysical properties.

2 | EXPERIMENT PROCEDURE

The detailed information about specimen preparation and property measurement of RE_3NbO_7 is provided in the Appendix S1.

3 | RESULTS AND DISCUSSION

Compared with the standard PDF cards, Figure 1A depicts that RE_3NbO_7 (RE=La, Nd, Sm, Eu, Gd) are ordered orthorhombic phase called weberite and Dy_3NbO_7 is disordered cubic phase called fluorite. Furthermore, the space group is Pnma for RE_3NbO_7 (RE=La, Nd, Sm, Eu), it is $C222_1$ for Gd_3NbO_7 and it is $Fm\bar{3}m$ for Dy_3NbO_7. Assuming that the lattice parameters of fluorite Dy_3NbO_7 are $a = b = c = a_1$, it is $a = \sqrt{2}\ a_1$, $b = 2a_1$ and $c = \sqrt{2}\ a_1$ for RE_3NbO_7 (RE = La, Nd, Sm, Eu) and it is $a = 2a_1$, $b = \sqrt{2}\ a_1$, and $c = \sqrt{2}\ a_1$ for Gd_3NbO_7. Figure 1B depicts that the main XRD peaks of RE_3NbO_7 shift to higher diffraction angle due to the lanthanum contraction, indicating that the lattice parameter decreases with the decreasing RE^{3+} ionic radius. Figure 1C depicts that the unit cell volume of RE_3NbO_7 shrinks with the decreasing RE^{3+} ionic radius and Dy_3NbO_7 with fluorite structure exhibits the minimum value. Figure 1D and F depict that Dy_3NbO_7 features broadening Raman spectrum due to the disordered atomic arrangement, which is evidently different from the rest RE_3NbO_7 with ordered weberite structure. The $F_{2\ g}$ Raman mode in Figure 1E derives from the Nb–O stretching mode, and the wave number increases with the decreasing RE^{3+} ionic radius due to the decreasing mean distance Nb–O.[19,23–25] In addition, the broadening Raman mode around 350 cm^{-1} in Figure 1D characters that the crystal structure order of RE_3NbO_7 decreases with the decreasing RE^{3+} ionic radius.

Figure 2 depicts that each RE_3NbO_7 crystallizes uniformly, and the grain boundary among various grains is obvious. In addition, the grain size of RE_3NbO_7 (RE = La, Nd, Sm) (5-20 μm) is evidently larger than RE_3NbO_7 (RE = Eu, Gd, Dy) (1-5 μm). The grain size relates to the sintering temperature, which is about 1600°C for RE_3NbO_7 (RE = La, Nd, Sm), and it is about 1650°C for RE_3NbO_7 (RE = Eu, Gd, Dy). The relatively high sintering temperature can reduce the sintering rate of TBC materials. The sintering temperature relates to RE^{3+} ionic radius, Navrotsky's research reveals that the enthalpy of formation from oxides becomes more exothermic with the increasing size of the RE^{3+} cation.[26] Herein, the sintering temperature of RE_3NbO_7 ceramics increases with the decreasing RE^{3+} ionic radius.[26] Minus pores are detected in RE_3NbO_7 and the relative density of these ceramics is as high as 98%. The Vickers hardness and fracture toughness are listed in Table 1. One can see that the highest hardness reaches 7.0 GPa, and the fracture toughness ranges from 0.8 to 1.5 MPa $m^{1/2}$. It is inferred that the hardness of RE_3NbO_7 increases with the decreasing inter-atomic distance.

Figure 3A depicts that the deformation variable of RE_3NbO_7 increases with the increasing temperature except Sm_3NbO_7, a sudden reduction of deformation variable is detected in Sm_3NbO_7. The deformation variable of RE_3NbO_7 increases with the decreasing RE^{3+} ionic radius, and the similar situation is observed in thermal expansion coefficients (TECs). Figure 3B depicts that the TECs of RE_3NbO_7 increase with the increasing temperature, except Sm_3NbO_7. The reduction of deformation variable and TECs of Sm_3NbO_7 should be due to the phase transition. Figure 3C depicts that the phase transition of Sm_3NbO_7 completes at 817°C and the similar situation is reported in Ref.[21,27] At 1200°C, the highest TECs ($11.0 \times 10^{-6}\ K^{-1}$) are detected in Dy_3NbO_7 as the TECs of RE_3NbO_7 increase with the decreasing RE^{3+} ionic radius. It is well-known that TECs increase with the decreasing crystal lattice energy, and crystal lattice energy decreases with the decreasing crystal structural order in fluorite-type ceramics.[28,29] The phase structure analysis indicates that the crystal structural order of RE_3NbO_7 decreases with the decreasing RE^{3+} ionic radius, which results in the increase of TECs. Besides, the highest TECs ($12.0 \times 10^{-6}\ K^{-1}$, 560°C) of RE_3NbO_7 during the whole test temperature are detected in Sm_3NbO_7. It will be significant for us to eliminate the phase transition and maintain the high TECs of Sm_3NbO_7 applied as TBCs.

Figure 3D depicts that the specific heat calculated by Neumann-Kopp rule of RE_3NbO_7 increases with the increasing temperature (0.3-0.5 J $g^{-1}\ K^{-1}$),[30] which is much lower than YSZ (0.4-0.7 J $g^{-1}\ K^{-1}$) and is similar with $Sm_2Zr_2O_7$ (0.3-0.6 J $g^{-1}\ K^{-1}$) from room temperature (RT) to 900°C. For comparison, compact yttria stabilized zirconia (YSZ) and $Sm_2Zr_2O_7$ (SmZr) bulk specimens have been synthesized via solid-state reaction. Figure 3E depicts that the thermal diffusivity of RE_3NbO_7 decreases with the increasing temperature (0.3-0.7 mm^2/s), which is much lower than YSZ (0.5-1.0 mm^2/s) and $Sm_2Zr_2O_7$ (0.4-0.9 mm^2/s) from RT to 900°C. In general, thermal diffusivity relates to the velocity acoustic and phonon mean free path. As velocity is almost temperature independent, the decreasing thermal diffusivity is owing to the decreasing

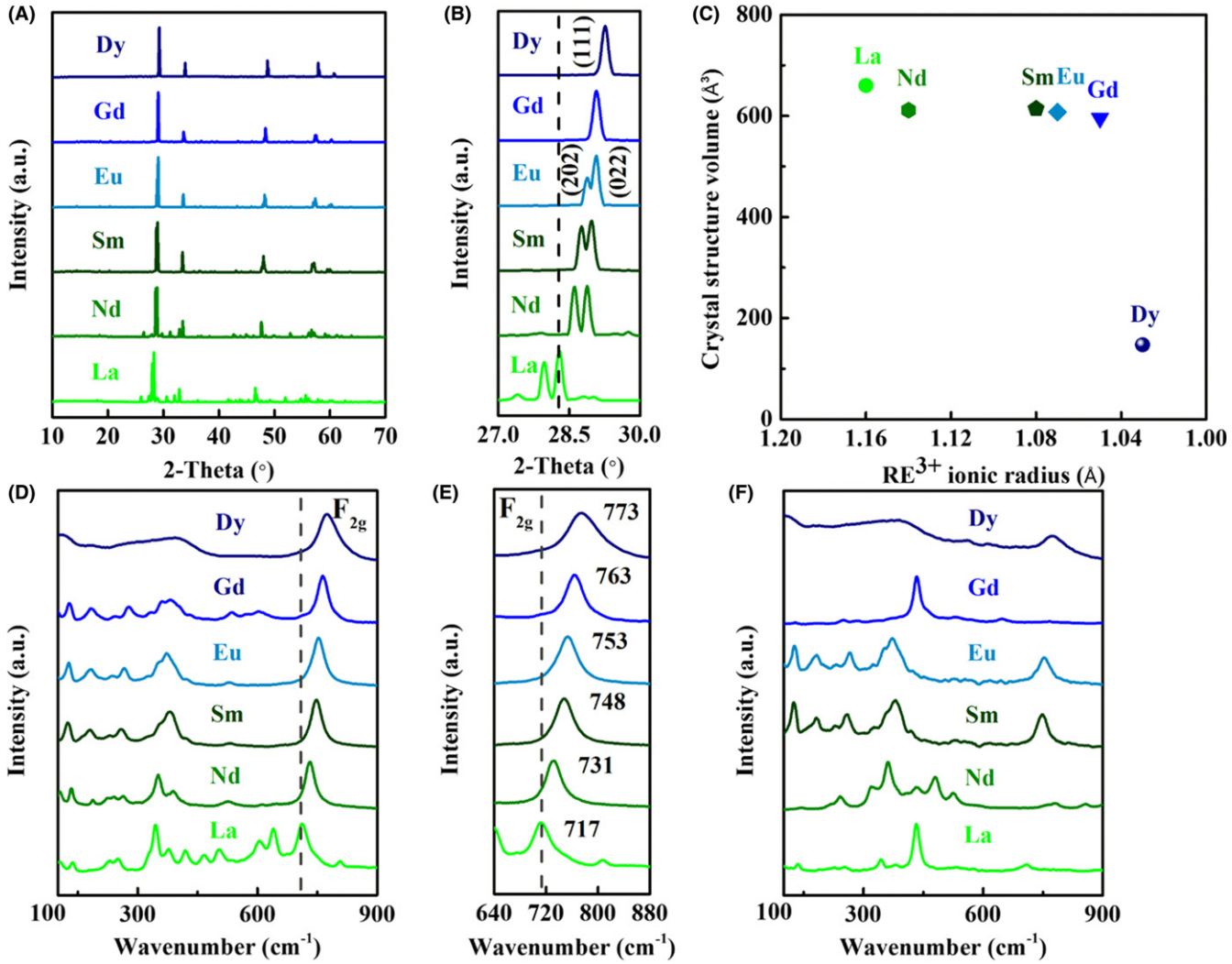

FIGURE 1 Phase characterization of RE_3NbO_7 (RE = La, Nd, Sm, Eu, Gd, Dy) ceramics; A, Normalized XRD, 10°≤2-Theta≤70°; B, Normalized XRD, 27°≤2-Theta≤30°; C, Crystal structure volume; D, Normalized Raman, 532 nm; E, Normalized F_{2g} Raman mode, 532 nm; F, Normalized Raman, 785 nm [Color figure can be viewed at wileyonlinelibrary.com]

phonon mean free path. Besides, the thermal diffusivity at low temperature of Dy_3NbO_7 is much lower than the rest. The disordered atom arrangement in fluorite Dy_3NbO_7 will increase the inharmonic lattice vibration, strengthen phonon scattering and then decrease thermal diffusivity.

Figure 3F depicts that RE_3NbO_7 exhibits extremely low thermal conductivity (1.0-1.8 W m^{-1} K^{-1}), which is much lower than YSZ (2.1-2.7 W m^{-1} K^{-1}) and $Sm_2Zr_2O_7$ (1.4-2.1 W m^{-1} K^{-1}) from RT to 900°C and it decreases with the increasing temperature. The temperature dependence of thermal conductivity is similar with thermal diffusivity of RE_3NbO_7 as the thermal is conducted via phonon in insulation materials. According to Debye's phonon gas theory, thermal conductivity can be reduced by phonon scattering when the thermal is conducted via phonon[31,32]:

$$k = 1/3 C_V l V_M \tag{1}$$

where V_M is the mean velocity acoustic, which is almost temperature independent; C_V is the specific heat and it approaches the limit value ($3k_B$) when the temperature is higher than the Debye temperature according to the Dulong-Petit rule.[33] Therefore, thermal conductivity (k) is dominated by the phonon mean free path l in RE_3NbO_7 and the low thermal conductivity derives from the short phonon mean free path. Phonon can be scattered by the complex crystal structure (l_c), grain boundary (l_b) and various lattice imperfections (l_l) (such as oxygen vacancy and the losing interatomic linkages).[33,34] Herein, the temperature-dependent phonon mean free path $l(f, T)$ with certain frequency (f) is[35,36]:

$$\frac{1}{l(f,T)} = \frac{1}{l_c} + \frac{1}{l_b} + \frac{1}{l_l} \tag{2}$$

Figure 2 depicts that the grain size of RE_3NbO_7 is 1-20 μm, which is several order of the phonon mean free

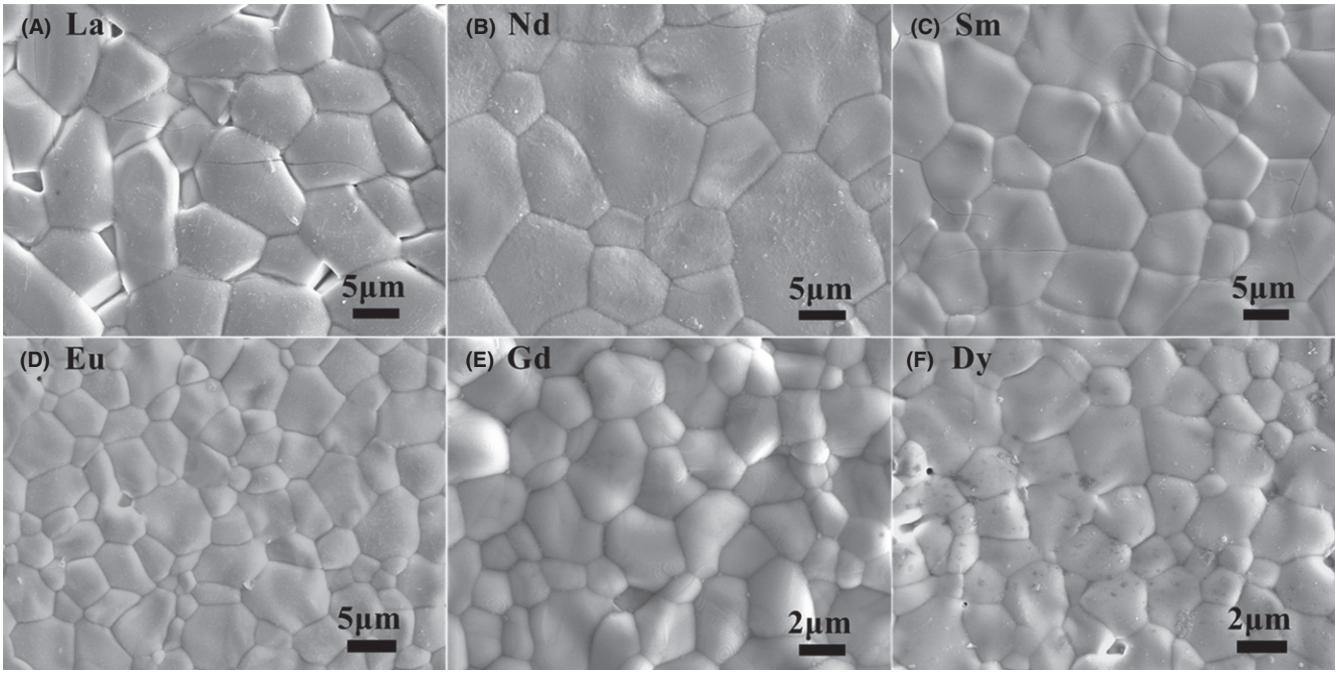

FIGURE 2 Typical microstructure of RE_3NbO_7 (RE = La, Nd, Sm, Eu, Gd, Dy) ceramics; A, La3NbO7; B, Nd3NbO7; C, Sm3NbO7; D, Eu3NbO7; E, Gd3NbO7; F, Dy3NbO7

TABLE 1 Vickers hardness (H_V/GPa) and fracture toughness (K_{IC}/MPa $m^{1/2}$) of RE_3NbO_7 (RE = La, Nd, Sm, Eu, Gd, Dy) ceramics

RE_3NbO_7	La_3NbO_7	Nd_3NbO_7	Sm_3NbO_7	Eu_3NbO_7	Gd_3NbO_7	Dy_3NbO_7
H_V	4.7	5.0	5.6	7.0	7.0	6.8
K_{IC}	0.8	1.1	1.4	1.5	1.5	1.4

path (nm). Furthermore, the influence of grain boundary scattering on phonon decreases dramatically with the increasing temperature and it can be omitted at elevated temperature.[37,38] Hence, the extremely low thermal conductivity of RE_3NbO_7 originates from the strong intrinsic crystal structure and lattice imperfection scattering. The crystal structures of RE_3NbO_7 derive from the prototype $A_4^{4+}O_8$ ($Fm\bar{3}m$) by the following process. Four tetravalent cations (A^{4+}) are displaced by 3 trivalent RE^{3+} and one pentavalent Nb^{5+}, and one oxygen vacancy is produced in each unit cell to maintain electrical neutrality.[20,39] The oxygen vacancy concentration is as high as 12.5% (1/8) in RE_3NbO_7, which is the strongest phonon scattering center among diverse lattice imperfections. The chemical formula of weberite RE_3NbO_7 is $A^{3+}A'^{3+}{}_2B^{5+}OO'{}_4O''{}_2\square$, when the chemical formula of fluorite RE_3NbO_7 ceramics is $A^{3+}{}_3B^{5+}O_7\square$ ($\square$ represents oxygen vacancy).[20,39] In addition, each Nb coordinates with 6 O atoms to form NbO_6 octahedron in weberite RE_3NbO_7, which is called the framework structure. The complex framework structure and high concentration of oxygen vacancy will lead to strong phonon scattering and decrease thermal conductivity.

The minimum thermal conductivity (1.0 W m^{-1} K^{-1}) of RE_3NbO_7 is detected in Sm_3NbO_7 (600°C) and Dy_3NbO_7 (25°C), which is attributed to the different reasons. The phase transition starts at 560°C and completes at 817°C according to the TECs and thermal conductivity of Sm_3NbO_7. During the phase transition, Sm_3NbO_7 ceramics with different space group (Pnma and $C222_1$, they are both subgroup of Cmcm) coexist, and Sm_3NbO_7 with Pnma space group is much more regular than the other one.[21,27] The phase transition should be responsible for the change of TECs and thermal conductivity of Sm_3NbO_7. The thermal conductivity of Dy_3NbO_7 increases slightly with the increasing temperature contributed to the increasing specific heat as the thermal diffusivity is almost temperature independent (Figure 3D and E). The thermal conductivity of Dy_3NbO_7 is also called the glass-like thermal conductivity as it approaches the value of amorphous limit, which roots in the unique fluorite crystal structure. The XRD result indicates a long-range average fluorite structure of Dy_3NbO_7, nevertheless, the local structure of fluorite Dy_3NbO_7 is different from the average fluorite structure. The local structural order is detected by Lopez-Conesa, the pyrochlore phase microdomains with size below the XRD sensitivity embeds in the average fluorite RE_3NbO_7.[20] Moreover, Siqueira et al report the existence of lower-symmetry nano-domains immerse in the average fluorite RE_3NbO_7 and the short-range structural

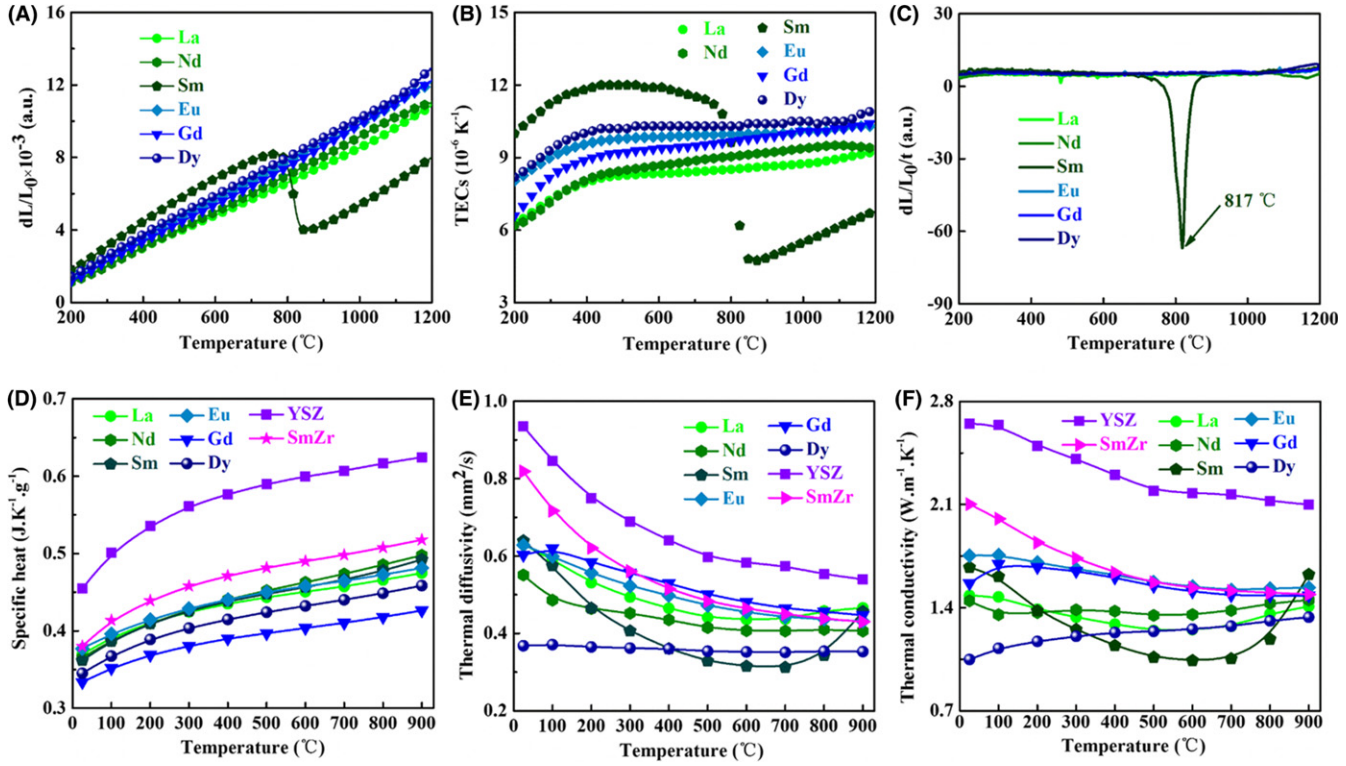

FIGURE 3 Thermophysical properties of RE_3NbO_7 (RE = La, Nd, Sm, Eu, Gd, Dy) ceramics; A, Deformation variable; B, Thermal expansion coefficients; C, Phase stability; D, Specific heat; E, Thermal diffusivity; F, Thermal conductivity [Color figure can be viewed at wile yonlinelibrary.com]

domains relate to the ordered arrangement of RE/Nb cations and/or oxygen vacancies.[19] Accordingly, it is believed that the glass-like thermal conductivity of fluorite Dy_3NbO_7 is dominated by the high concentration of oxygen vacancy and local structural order.

4 | CONCLUSION

The order-disorder phase transition occurs in RE_3NbO_7 (RE = La, Nd, Sm, Eu, Gd, Dy) synthesized via solid-state reaction attributed to the lanthanide contraction. Dy_3NbO_7 is disordered cubic fluorite structure when the rest is ordered orthorhombic weberite structure. The TECs increase with the decreasing RE^{3+} ionic radius and the maximum value at 1200°C reaches 11.0×10^{-6} K^{-1}, as the crystal lattice energy of RE_3NbO_7 decreases with the decreasing crystal structural order. The framework crystal structure and high concentration of oxygen vacancy (12.5%) lead to strong phonon scattering, which cause the extremely low thermal conductivity (1.0 W m^{-1} K^{-1}) of RE_3NbO_7. Local structural order exists in the long-range average disordered fluorite Dy_3NbO_7, which is the extra phonon scattering center and results in the glass-like thermal conductivity. As for mechanical properties, the highest hardness and fracture toughness reach 7.0 GPa and 1.5 MPa $m^{1/2}$, respectively. The high TECs, excellent high-temperature phase stability and extremely low thermal conductivity claim that RE_3NbO_7 ceramics are potential TBC materials.

ACKNOWLEDGMENTS

This research is under the support of the Natural Science Foundation of China (No. 51762028) and the young-talent support programs of Kunming University of Science and Technology (No. 11504146).

ORCID

Lin Chen http://orcid.org/0000-0002-4730-2845
Peng Wu http://orcid.org/0000-0001-7031-410X

REFERENCES

1. Clarke DR, Phillpot SR. Thermal barrier coating materials. Mater Today. 2005;8:22–9.
2. Padture NP, Gell M, Jordan EH. Thermal barrier coatings for gas-turbine engine applications. Science. 2002;296:280–4.
3. Clarke DR, Levi CG. Materials design for the next generation thermal barrier coatings. Annu Rev Mater Res. 2003;33:383–417.

4. Chen L, Yang GJ. Epitaxial growth and cracking of highly tough 7YSZ splats by thermal spray technology. J Adv Ceram. 2018;7:17–29.
5. Ren XR, Pan W. Mechanical properties of high-temperature-degraded yttria-stabilized zirconia. Acta Mater. 2014;69:397–406.
6. Schlichting KW, Padture NP, Klemens PG. Thermal conductivity of dense and porous yttria-stabilized zirconia. J Mater Sci. 2001;36:3003–10.
7. Siebert B, Funke C, Vassen R, Stöver D. Changes in porosity and Young's modulus due to sintering of plasma sprayed thermal barrier coatings. J Mater Process Tech. 1999;93:217–23.
8. Cao XQ, Vaben R, Stover D. Ceramic materials for thermal barrier coatings. Mater Sci Eng A-Struct. 1998;245:143–9.
9. Zhang WW, Li GR, Zhang Q, Yang GJ. Comprehensive damage evaluation of localized spallation of thermal barrier coatings. J Adv Ceram. 2017;6:230–9.
10. Wu J, Wei XZ, Padture NP, Klemens PG, Gell M, Osendi MI, et al. Low-thermal-conductivity rare-earth zirconates for potential thermal-barrier-coating applications. J Am Ceram Soc. 2002;85:3031–5.
11. Wan CL, Zhang W, Wang YF, Qu ZX, Du AB, Wu RF, et al. Glass-like thermal conductivity in ytterbium-doped lanthanum zirconate pyrochlore. Acta Mater. 2010;58:6166–72.
12. Cao XQ, Vassen R, Fischer W, Tietz F, Jungen W, Stover D. Lanthanum-cerium as a thermal-barrier-coating material for high-temperature applications. Adv Mater. 2003;17:1438–42.
13. Wu P, Hu MY, Chong XY, Feng J. The glass-like thermal conductivity ZrO_2-Dy_3TaO_7 ceramic for promising thermal barrier coating application. Appl Phys Lett. 2018;112:131903.
14. Zhang H, Feng Y, Chen X, Zhang HS, Liu YX, Tang A, et al. Thermal properties of La_3TaO_7 and La_2AlTaO_7 oxides. Ceram Int. 2017;43:755–9.
15. Wang J, Zhou Y, Chong XY, Zhou R, Feng J. Microstructure and thermal properties of $RETaO_4$ (RE=Nd, Eu, Gd, Dy, Er, Yb, Lu) as promising thermal barrier coating materials. Scripta Mater. 2017;126:24–8.
16. Ren XR, Wan CL, Zhao M, Yang J, Pan W. Mechanical and thermal properties of fine-grained quasi-eutectoid $(La_{1-x}Yb_x)_2Zr_2O_7$ ceramics. J Eur Ceram Soc. 2015;35:3145–54.
17. Yang J, Wan CL, Zhao M, Shahid M, Pan W. Effective blocking of radiative thermal conductivity in $La_2Zr_2O_7/LaPO_4$ composites for high temperature thermal insulation applications. J Eur Ceram Soc. 2016;36:3809–14.
18. Wan CL, Qu ZX, Du AB, Pan W. Influence of B site substituent Ti on the structure and thermophysical properties of $A_2B_2O_7$-type pyrochlore $Gd_2Zr_2O_7$. Acta Mater. 2009;57:4782–9.
19. Siqueira KPF, Soares JC, Granado E, Bittar EM, Paula AM, Moreira RL, et al. Synchrotron X-ray diffraction and Raman spectroscopy of Ln_3NbO_7 (Ln=La, Pr, Nd, Sm-Lu) ceramics obtained by molten-salt synthesis. J Solid State Chem. 2014;209:6368.
20. Lopez-Conesa L, Rebled JM, Chambrier MH, Boulahya K, González-Calbet JM, Braida MD, et al. Local structure of rare earth niobates (RE_3NbO_7, RE=Y, Er, Yb, Lu) for proton conduction applications. Fuel Cells. 2013;1:29–33.
21. Klimenko AN, Kozlov YS, Sergeev VS, Pastukhov EA. High temperature phase transitions in rare earth element niobates R_3NbO_7. Thermochim Acta. 1992;209:331–8.
22. Cai L, Nino JC. Structure and dielectric properties of Ln_3NbO_7 (Ln = Nd, Gd, Dy, Er, Yb and Y). J Eur Ceram Soc. 2007;27:3971–6.
23. Chesnaud A, Braida MD, Estrade S, Peiród F, Tarancónf A, Morataf A, et al. High-temperature anion and proton conduction in RE_3NbO_7 (RE=La, Gd, Y, Yb, Lu) compounds. J Eur Ceram Soc. 2015;35:3051–61.
24. Poulsen FW, Glerup M, Holtappels P. Structure. Raman spectra and defect chemistry modelling of conductive pyrochlore oxides. Solid State Ionics. 2000;135:595–602.
25. Cai JG, Raptis C, Raptis YS, Anastassakis E. Temperature dependence of Raman scattering in stabilized cubic zirconia. Phys Rev B. 1995;51:201–9.
26. Mielewczyk-Gryn A, Navrotsky A. Enthalpies of formation of rare earth niobates, RE_3NbO_7. Am Mineral. 2015;100:1578–83.
27. Hinatsu Y, Doi Y. Studies on phase transition temperature of rare earth niobates Ln_3NbO_7 (Ln=Pr, Sm, Eu) with orthorhombic fluorite-related structure. Solid State Sci. 2017;68:19–24.
28. Qu ZX, Wan CL, Pan W. Thermophysical properties of rare-earth stannates: effect of the pyrochlore structure. Acta Mater. 2012;60:2939–49.
29. Kennedy BJ, Hunter BA, Howard CJ. Structural and bonding trends in tin pyrochlore oxides. J Solid State Chem. 1997;130:58–65.
30. Leitner J, Chuchvalec P, Sedmidubsky D, Strejc A, Abrman P. Estimation of heat capacities of solid mixed oxides. Thermochim Acta. 2003;395:1074–84.
31. Kittle C. *Introduction to solid state physics*. New York, NY: Wiley; 1996.
32. Berman R. *Thermal conduction in solid*. Oxford, UK: Clarendon Press; 1976.
33. Beekman M, Cahill DG. Inorganic crystal with glass-like and ultra-low thermal conductivities. Cryst Res Technol. 2017;52:1700114.
34. Padture NP, Klemens PG. Low thermal conductivity in garnets. J Am Ceram Soc. 1997;80:1018–20.
35. Klemens PG. The scattering of low-frequency lattice waves by static imperfections. Proc Phys Soc A. 1955;68:1113–28.
36. Callaway J, Baeyer HC. Effect of point imperfection on lattice thermal conductivity. Phys Rev. 1960;120:1149–54.
37. Braginsky L, Shklover V, Hofmann H, Bowen P. High-temperature thermal conductivity of porous Al_2O_3 nanostructures. Phys Rev B. 2004;70:134201.
38. Chen L, Jiang YH, Chong XY, Feng J. Synthesis and thermophysical properties of $RETa_3O_9$ (RE=Ce, Nd, Sm, Eu, Gd, Dy, Er) as promising thermal barrier coatings. J Am Ceram Soc. 2018;101:1266–78.
39. Siqueira KPF, Borges RM, Granad E, Malard LM, Paula AM, Moreira RL, et al. Crystal structure of fluorite-related Ln_3SbO_7 (L=La–Dy) ceramics studied by synchrotron X-ray diffraction and Raman scattering. J Solid State Chem. 2013;203:326–32.

SUPPORTING INFORMATION

Additional supporting information may be found online in the Supporting Information section at the end of the article.

How to cite this article: Chen L, Wu P, Song P, Feng J. Potential thermal barrier coating materials: RE_3NbO_7 (RE=La, Nd, Sm, Eu, Gd, Dy) ceramics. *J Am Ceram Soc*. 2018;101:4503–4508. https://doi.org/10.1111/jace.15798